

# RSC Advances



This is an *Accepted Manuscript*, which has been through the Royal Society of Chemistry peer review process and has been accepted for publication.

*Accepted Manuscripts* are published online shortly after acceptance, before technical editing, formatting and proof reading. Using this free service, authors can make their results available to the community, in citable form, before we publish the edited article. This *Accepted Manuscript* will be replaced by the edited, formatted and paginated article as soon as this is available.

You can find more information about *Accepted Manuscripts* in the [Information for Authors](#).

Please note that technical editing may introduce minor changes to the text and/or graphics, which may alter content. The journal's standard [Terms & Conditions](#) and the [Ethical guidelines](#) still apply. In no event shall the Royal Society of Chemistry be held responsible for any errors or omissions in this *Accepted Manuscript* or any consequences arising from the use of any information it contains.

## Preparation and electrochemical capacitance of graphene/titanium nitride nanotube array

Fang Tian<sup>a</sup>, Yibing Xie<sup>a,b</sup>, Hongxiu Du<sup>a,b</sup>, Yingzhi Zhou<sup>a</sup>, Chi Xia<sup>a,b</sup>, and Wei Wang<sup>a,b</sup>

<sup>a</sup> School of Chemistry and Chemical Engineering, Southeast University, Nanjing 211189, China

<sup>b</sup> Suzhou Research Institute of Southeast University, Suzhou 215123, China

**Abstract:** Two kinds of graphene composite electrode materials were synthesized on the substrate of titanium nitride nanotube array (TiN NTA) and nickel foam (NF) by simple adsorption-reduction process, forming graphene/titanium nitride nanotube array (G/TiN NTA) and graphene/nickel foam (G/NF). Both the chemical reduction method and the thermal reduction method were used to convert graphene oxide into graphene, forming G/TiN NTA and thermal reduction graphene/titanium nitride nanotube array (TRG/TiN NTA). The morphology and microstructure of G/TiN NTA, G/NF and TRG/TiN NTA were characterized by scanning electron microscopy, Raman spectra and X-ray diffraction analysis. The electrochemical performances of G/TiN NTA, G/NF and TRG/TiN NTA were investigated by electrochemical impedance spectroscopy, cyclic voltammetry and galvanostatic charge/discharge measurements. The specific capacitance of G/NF and G/TiN NTA was 198.7 F g<sup>-1</sup> and 333.7 F g<sup>-1</sup> at a current density of 1 A g<sup>-1</sup> on the mass of graphene, respectively. TiN NTA was more suitable to act as a substrate material of graphene composite electrode to achieve higher capacitance performance for G/TiN NTA. Additionally, the specific capacitance of G/TiN NTA and TRG/TiN NTA were 230.7 F g<sup>-1</sup> and 197.9 F g<sup>-1</sup> at a current density of 4 A g<sup>-1</sup>, respectively. It indicated the chemical reduction method was effective to produce graphene composite electrode with higher capacitive performance. An all-solid state flexible supercapacitor was also constructed using two symmetric electrodes of G/TiN NTA and a gel electrolyte of polyvinyl alcohol-potassium hydroxide-potassium iodide, showing energy density of 34.2 Wh kg<sup>-1</sup> and power density of 11.3 kW kg<sup>-1</sup>.

**Keywords:** Graphene; Titanium nitride; Nanotube array; Electrochemical capacitance

## 1 Introduction

The demand for electrical energy has significantly increased with the rapid growth of the global economy and population. Great interest is stimulated in exploring advanced storage devices to meet the requirements for future electrochemical power sources and reliable energy storage system. Preparing good-performance and well-synthesized nanostructure electrode material is urgent to enhance the energy and power density, efficiency and durability of supercapacitors<sup>1-3</sup>.

Graphene, an atom thick graphite sheet, has attracted many researchers because of its high surface area, excellent electronic conductivity and mechanical strength<sup>4, 5</sup>. Its unique two-dimensional structure makes it have excellent chemical and physical properties. It has wide potential applications in nanoelectronics, energy storage and conversion, chemical and biological sensors, composite materials and biotechnology<sup>6, 7</sup>. To exploit the potential of graphene-based

materials for wide applications, many efforts have been made to fabricate various graphene architectures, and a considerable progress has been achieved<sup>8-10</sup>. In the process of reduction of graphene oxide, many defects can be produced. These defects may lead to decrease of electron transporting ability between graphene sheets. Thereby, different substrate materials are used to enhance the electrical conductive ability between the graphene sheets. In addition, graphene can agglomerate during the reduction of graphene oxide (GO) on account of stacked along the direction (c-axis) perpendicular to the substantial loss of oxygen containing groups, which can low the electrostatic repulsions between graphene oxide sheets<sup>11</sup>. High conductivity materials are exigent of being employed to enhance the electrical transport ability of graphene sheets. The highly ordered nanotube array materials with high surface area are usually regarded as very suitable substrate materials for various electrochemical applications<sup>12,13</sup>. Transition metal nitrides have been an appealing class because of their low cost, high molar density and superior chemical resistance<sup>14</sup>. TiN is emerging as a new and promising electrode material due to its high thermal chemical stability and low electrical resistivity<sup>15-18</sup>. Several attempts have been carried out to enhance the conductivity and prevent the aggregation of graphene by using TiN<sup>19</sup>. The 3-dimensional TiN NTA has a larger surface area, stronger adsorption capacity and faster electron transfer capability<sup>20,21</sup>. Its tubular channels can offer a rigid support structure to permit a feasible loading of electroactive materials. The well-aligned nanotubular structure can also provide more available spaces for electrochemical reactions.

In this study, In this study, G/TiN NTA and G/NF electrodes were prepared to investigate the effects of different substrate materials of titanium nitride nanotube array (TiN NTA) and nickel foam (NF) on the capacitance performance of graphene. G/TiN NTA and TRG/TiN NTA electrodes were prepared to investigate the influence of chemical reduction and thermal reduction methods on the capacitance performance of graphene. The nickel foam was generally used as electrode substrate material, which was applied to compare the titanium nitride nanotube array as a new kind of electrode substrate. In addition, An all-solid state flexible supercapacitor was also constructed using G/TiN NTA electrode to investigate its capacitance performance.

## 2 Experimental details

### Preparation of graphene oxide (GO)

GO was prepared by oxidation of natural graphite powder according to a modified Hummers' method<sup>22-24</sup>. In brief, 3.0 g graphite and 1.5 g sodium nitrate was mixed and added to 70 ml concentrated sulfuric acid under vigorous stirring, and then the mixture was cooled to 0°C in an ice bath. During vigorous stirring, potassium permanganate (9.0 g) was added slowly to keep the temperature of the suspension less than 20°C. Afterwards, the reaction system was transferred to a 38°C oil bath. Then, 140 ml of deionized water was added and stirred continuously for 15 minutes. Thereafter, 500 ml of deionized water and 20 ml of 30% H<sub>2</sub>O<sub>2</sub> (at a very slow speed) was added. The color of the solution changed from brown to yellow. The mixture was filtered and washed with 250 ml HCl aqueous solution (1:10) to remove metal ions followed by washing with deionized water and centrifugation to remove the acid. At last, the resulting solid was dispersed in water by ultrasonic treatment about 1 h to acquire a GO aqueous dispersion (0.5 wt%).

### Preparation of G/TiN and TRG/TiN NTA electrodes

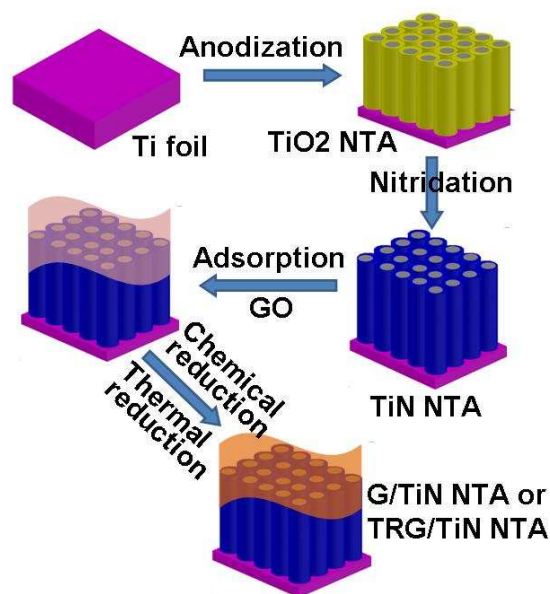


Fig. 1 A schematic illustration of the preparation of G/TiN NTA or TRG/TiN NTA electrodes

Fig. 1 illustrates the fabricating process of G/TiN NTA. TiO<sub>2</sub> nanotube arrays were formed by the anodization of metallic Ti at 60 V for 3 hours in ethylene glycol, distilled water and NH<sub>4</sub>F electrolyte solution. Subsequently, TiN NTA was obtained by annealing treatment of TiO<sub>2</sub> nanotube arrays in ammonia atmosphere at 900°C for 1 hour. GO is a highly effective adsorbent due to its large amounts of hydroxyl and epoxy groups. TiN NTA has large amounts of accessible

surface area. Accordingly, GO can well adsorb on the surface of TiN NTA by simply immersing TiN NTA in GO solution<sup>25</sup>. In virtue of the high adsorption capacity of GO, TiN NTA was then immersed in the obtained 0.5 wt% GO aqueous dispersion for 4 hours to adsorb a certain amount of GO. Two kinds of methods were used to reduce GO/TiN NTA electrode. The GO/TiN NTA electrode was reduced for 4 hours at 95°C by hydrazine hydrate, washed with deionized water and then dried to obtain the G/TiN NTA electrode. Alternatively, the GO/TiN NTA electrode was reduced for 3 hours by annealing at 600°C in argon atmosphere and the TRG/TiN NTA electrode was obtained.

#### **Preparation of G/NF composite electrode**

GO/NF composite electrode was obtained by immersing nickel foam in 0.5 wt% GO aqueous dispersion for 4 hours to adsorb a certain amount of GO solution. Then GO/NF electrode was reduced for 4 hours at 95°C by moderate hydrazine. Finally, it was washed with deionized water and then dried to obtain the G/NF electrode.

#### **Preparation of polyvinyl alcohol-potassium hydroxide-potassium iodide gel electrolyte**

Polyvinyl alcohol, potassium hydroxide, potassium iodide and ethylene glycol with a mass ratio of 3: 2: 2: 1 were dissolved in deionized water and stirred at 80°C for 2 h. The mixed solution was continuously agitated until to form a homogeneous liquid. The obtained solution of polyvinyl alcohol-potassium hydroxide-potassium iodide was placed in a vacuum oven at 60°C to evaporate excess water. Finally, an all-solid state polyvinyl alcohol-potassium hydroxide-potassium iodide gel electrolyte was obtained. Flexible supercapacitor was constructed using two electrodes of G/TiN NTA and polyvinyl alcohol-potassium hydroxide-potassium iodide gel electrolyte<sup>26</sup>.

#### **Characterization**

The surface morphology and microstructure of TiN NTA, TRG/TiN NTA and G/TiN NTA electrodes had been investigated using a scanning electron microscope (SEM, Hitachi S-3000N). Raman spectrum was measured to investigate SERS substrates using a Renishaw Invia Reflex System Raman spectrometer. The excitation wavelength was 785 nm. The 50\* objective lens was used to focus the laser light on the samples. The laser power was 0.1%, and integration time for each sample was 10 s. X-ray diffraction (XRD) patterns of TiN NTA and G/TiN NTA were

recorded using a X-ray diffractometer (PW3040/60 X' pert PRO) with Cu K radiation ( $\lambda=1.54178$  Å) operating at 40 kV and 40 A.

Electrochemical measurements were carried out using a CHI760D instrument at room temperature. Cyclic voltammetry (CV) curves at different scan rates, respectively. Galvanostatic charge/discharge curves were measured at different current densities, respectively.

Electrochemical impedance spectroscopy (EIS) of G/TiN NTA and G/NF electrodes was performed using an electrochemical workstation (IM6e, Zahner Elektrik). Measurements were carried out with a disturbing voltage of 5 mV over a frequency range of 0.01Hz–100 kHz at a circuit voltage of 0.059V. All simulations were performed using Z-view software.

### 3 Results and discussion

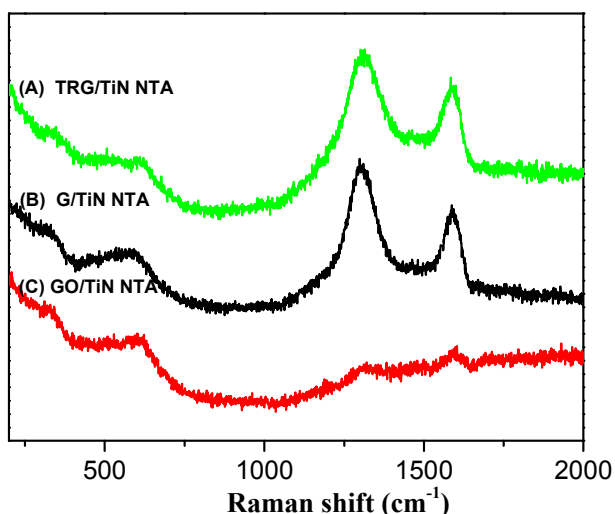


Fig. 2 Raman spectra of (A) TRG/TiN NTA, (B) G/TiN NTA and (C) GO/TiN NTA electrodes.

The G/TiN NTA, GO/TiN NTA and TRG/TiN NTA electrodes are further studied by Raman spectroscopy, which is a powerful tool for getting information on vibrational and rotational and studying the structure of molecular. The D band indicates occurrence of the  $sp^2$  carbon, which is associated with the structural defects or partially disordered structures of graphitic domains. While the G band corresponds to the zone center  $E_{2g}$  mode and related to in-plane band-stretching motion of  $sp^2$  carbon domain<sup>27, 28</sup>. Fig. 2 shows Raman spectra of G/TiN NTA, GO/TiN NTA and TRG/TiN NTA electrodes, respectively. The peaks at  $224\text{ cm}^{-1}$  and  $316\text{ cm}^{-1}$  are corresponding to TiN Raman scattering, which are caused by acoustical phonons<sup>29</sup>. The value of  $I_D/I_G$  (intensity

ratio of D and G band) represents the degree of disorder and average of the  $sp^2$  domain. The D band (peak at around  $1311\text{ cm}^{-1}$ ) is stronger than the G (peak at  $1587\text{ cm}^{-1}$ ), indicating the presence of substantial disordered structure and a large amount of defects in graphene (Fig. 2A and B). The intensity ratio of  $I_D/I_G$  of G/TiN NTA and GO/TiN NTA are 1.22 (Figure 2B) and 0.56 (Fig. 2C), respectively. The value of  $I_D/I_G$  is increased when GO was reduced into graphene by moderate hydrazine. Generally, the large amounts of hydroxyl and epoxy groups presented in graphene oxide can decrease the relative amount of six-fold aromatic rings and diminish the intensity of the D band. Such decrease ascribed to the low electrical conductivity of the unreduced graphene oxide. Most of those oxygenated groups are eliminated after chemical reduction. A method of thermal reduction was used to obtain TRG/TiN NTA electrode at  $600^\circ\text{C}$  for 3 hours. The intensity ratio of  $I_D/I_G$  of TRG/TiN NTA is 1.12 (Figure 2A). Compared with the value of  $I_D/I_G$  in Figure 2A and C, we drew a conclusion that GO was able to be reduced at  $600^\circ\text{C}$ .

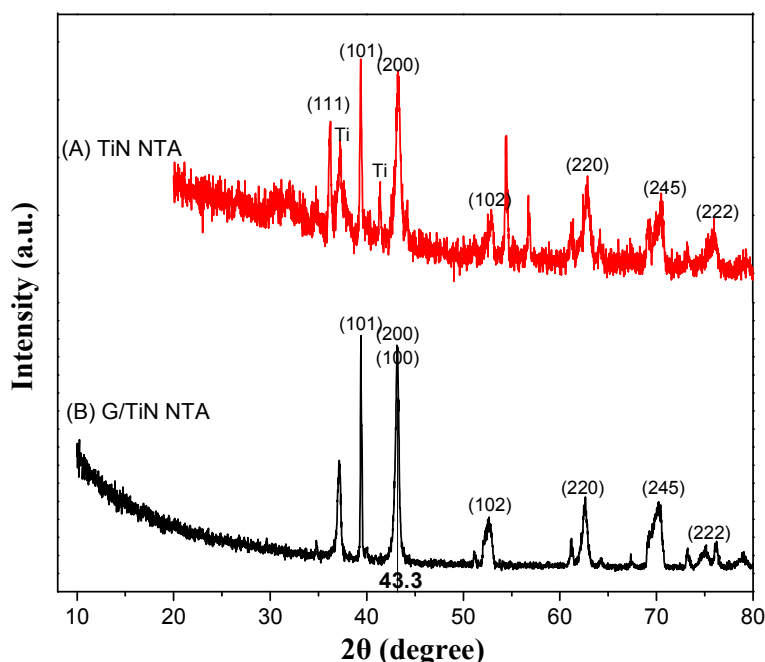
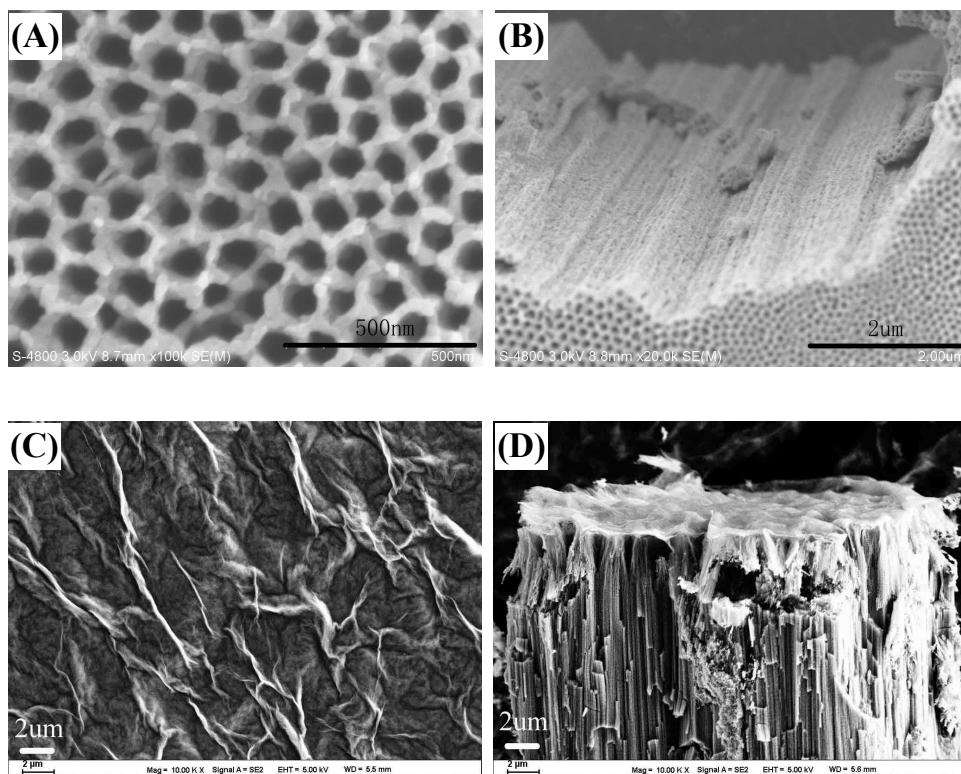


Fig. 3 XRD patterns of (A) TiN NTA and (B) G/TiN NTA electrodes.

The crystalline phase of TiN NTA and G/TiN NTA was analyzed by XRD, as shown in Fig. 3. Diffraction peaks at  $36.8^\circ$ ,  $39.2^\circ$ ,  $43.3^\circ$ ,  $52.6^\circ$ ,  $62.6^\circ$ ,  $70.2^\circ$ , and  $75.0^\circ$ , were ascribed to crystal planes of (111), (101), (200), (102), (110), (245), and (222), respectively by referring to JCPDS 38-1420 and 41-1352, which were assigned to characteristic diffraction peaks of osbornite phase TiN<sup>19</sup>. Other diffraction peaks were ascribed to titanium foil (see Fig. 3A). Concerning G/TiN NTA, the similar diffraction peaks were observed due to the crystal plane peaks of osbornite phase

TiN. The weak characteristic diffraction peak of graphene at  $43.3^\circ$  (crystal plane (100)) was completely overlapped with the peak (crystal plane (200)) of TiN (see Fig. 3B)<sup>30</sup>. Obviously, the osbornite phase TiN NTA shows a cubic crystal structure. The crystal structure of osbornite phase TiN keeps unchanged after the GO reduction process. It is well known that GO consists of various different types of oxygen functional groups such as hydroxyl, carbonyl, epoxide, lactone, or ether groups. Although the full mechanisms of GO reduction have not been clear yet, the reduction process involves the removal of the above oxygen functional groups. GO can be well converted into the reduced graphene oxide through chemical reduction process. Accordingly, the reduced graphene oxide keeps less defects on its structure in comparison with GO. The obtained G/TiN NTA electrode good crystal structure.



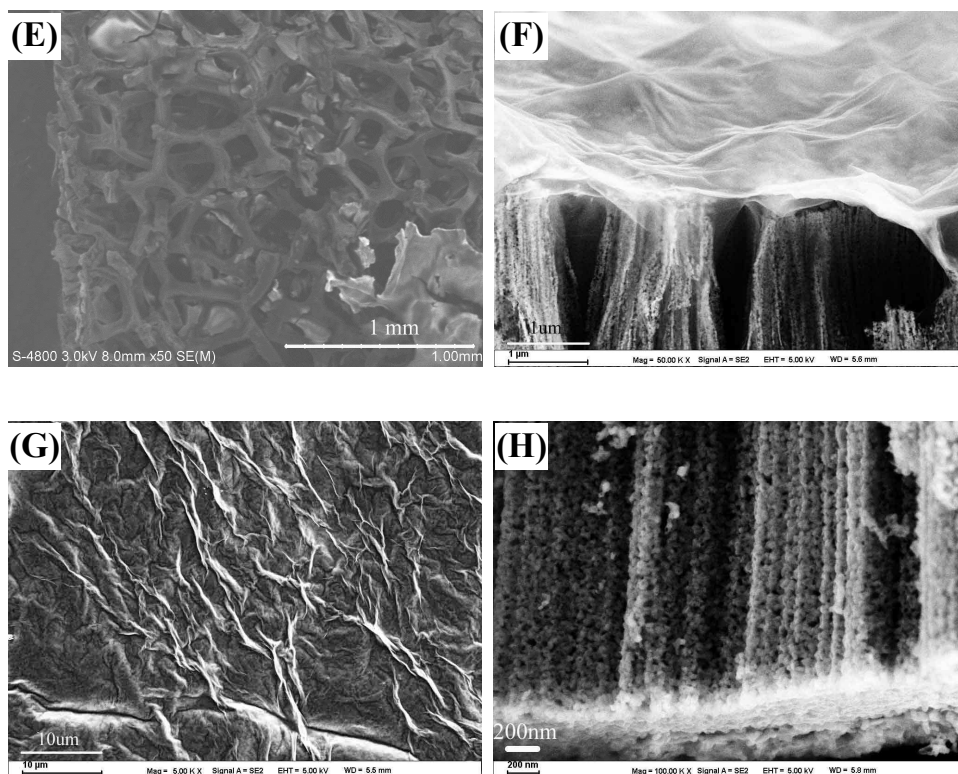


Fig. 4 (A) Top-view and (B) cross-section view SEM images of TiN NTA; (C) top-view and (D) cross-section view SEM images of G/TiN NTA electrode; (E) top-view SEM images of G/NF electrode; (F) cross-section view SEM images of TRG/TiN NTA electrode; (G) top-view and (H) cross-section view SEM images of G/TiN NTA after 1000 cycles.

Fig. 4 shows the SEM images of TiN NTA, G/NF, TRG/TiN NTA and G/TiN NTA electrodes. TiN NTA kept vertically oriented and highly ordered nanotube alignment, whose inner diameter was less than 120 nm and wall thickness was 30-55 nm. The total length of TiN nanotubes was approximately 5.0  $\mu\text{m}$  (Fig. 4A and B). Fig. 4C shows that the lamellar graphene was uniformly distributed on TiN NTA. Fig. 4D and F are cross-view SEM images of G/NF and TRG/NF electrodes. Graphene was uniformly adsorbed on TiN NTA and the length of TiN nanotubes is the same as before. Fig. 4E shows that lamellar graphene was also formed on nickel foam, presenting an obvious aggregation. The main reason may be that nickel foam has much smaller surface area than that of TiN NTA and the adsorption ability between graphene and nickel foam is not so strong. Fig. 4G and H are top-view and cross-section view SEM images of G/TiN NTA after 1000 cycles. TiN NTA could still maintain an initial structure of tubular framework after 1000 cycles.

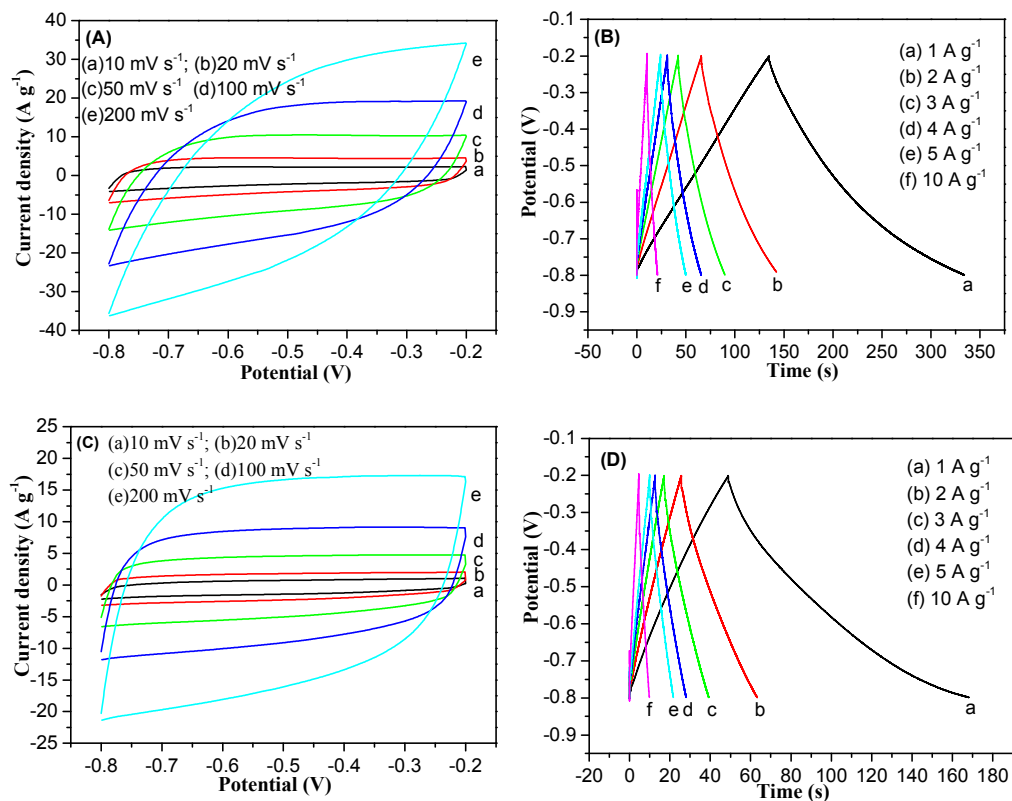


Fig. 5 Cyclic voltammetry curves of (A) G/TiN NTA and (C) G/NF electrode; Galvanostatic charge/discharge curves of (B) G/TiN NTA and (D) G/NF electrode.

Fig. 5 shows the cyclic voltammetry and galvanostatic charge/discharge curves of G/TiN NTA and G/NF electrodes in 1.0 M KOH electrolyte solution. Cyclic voltammetry measurements were performed in a potential range from -0.8 to -0.2 V at scan rates of 10, 20, 50, 100, and 200  $\text{mV s}^{-1}$ , respectively. The G/TiN NTA electrode showed symmetrical characteristic at the axis of zero current and approached the quasi-rectangular shape over a full scan range (Fig. 5A). The rectangular shape indicates that near ideal capacitive property even the scanning rate reach to 200  $\text{mV s}^{-1}$ .

The current response enhanced when scan rate increased. The cyclic voltammetry curves of G/NF electrode also showed a quasi-rectangular shape. The shape of these cyclic voltammetry curves remained unchanged when the scan rate was increased from 10 to 200  $\text{mV s}^{-1}$ , indicating good capacitive behavior and high-rate capability of G/NF electrode. However, G/TiN NTA electrode shows higher current response than G/NF electrode in 1.0 M KOH solution. Compared with G/NF electrode, the higher current may be attributed to the structure of the G/TiN NTA electrode, which is more accessible to the fast diffusion of electrolyte ions. This is mainly ascribed

to TiN NTA, which offered a high surface area and improved the electronic transmission between graphene sheets.

The specific capacitance (C), specific energy (E) and specific power (P) densities are calculated from the following equations<sup>41</sup>.

$$C = Q/(\Delta V \times m) = (I \times t) / (\Delta V \times m) \quad (1)$$

$$E = (I \times t \times \Delta V) / 2m = [C \times (\Delta V)^2] / 2 \quad (2)$$

$$P = (I \times \Delta V) / 2m \quad (3)$$

Where I is the discharge current (A); t,  $\Delta V$  and m are discharge time (s), potential window (V) and mass of active material (g), respectively.

The charge/discharge curves of the G/TiN NTA and G/NF electrodes at different current densities in 1.0 M KOH electrolyte are shown in Fig. 5B and D. The specific capacitance of G/TiN NTA and G/NF electrodes reached 333.67 F g<sup>-1</sup> and 198.67 F g<sup>-1</sup> at the current density of 1.0 A g<sup>-1</sup> on the mass of graphene, respectively. Table 1 lists the specific capacitance of G/TiN NTA and G/NF electrodes at different current densities in 1.0 M KOH solution. The G/TiN NTA electrode had higher specific capacitance than that of G/NF electrode at the same current density. This is mainly ascribed to TiN NTA, whose three-dimensional tubular structure could provide larger contact area and stronger adsorption ability than nickel foam. Compared with G/NF electrode, the G/TiN NTA electrode had more conducive to fast transfer of electrons and effectively improved the electronic transmission capacity and greatly shortened the diffusion path of ions.

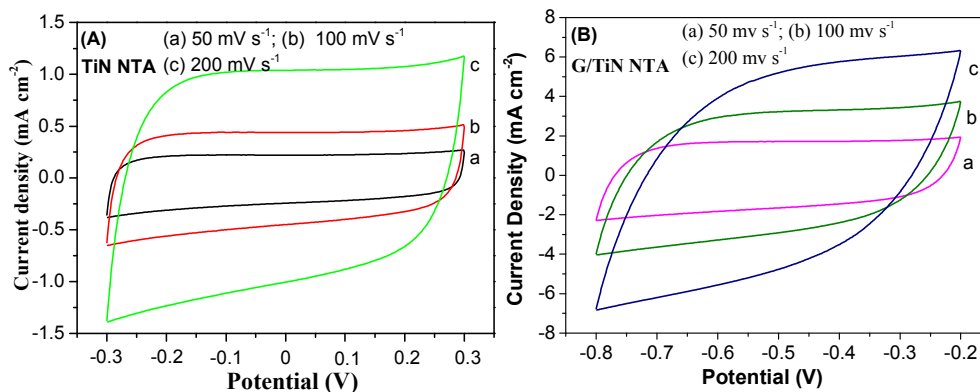
Table 1 Specific capacitance of G/TiN NTA and G/NF electrodes at the different current densities.

Current density (A g <sup>-1</sup> )	1	2	3	4	5	10
Specific capacitance (F g <sup>-1</sup> ) of G/TiN NTA	333.7	261.7	238.5	231.5	216.5	177.8
Specific capacitance (F g <sup>-1</sup> ) of G/NF	198.7	150.4	110.9	102.9	97.4	86.3

Fig. 6A and B show cyclic voltammetry curves of TiN NTA and G/TiN NTA electrodes at scan rates of 50, 100 and 200 mV s<sup>-1</sup>, respectively. The current response of both electrodes was enhanced when scan rate increased. The cyclic voltammetry curves of TiN NTA exhibited a symmetrical characteristic at the axis of zero current and approached the quasi-rectangular shape over a full scan range in the applied potential from -0.3 to 0.3 V. TiN NTA electrode showed an ideal electric double layer capacitance. The cyclic voltammetry curves of G/TiN NTA electrode

also had a similar quasi-rectangular shape at a low scan rate, showing an ideal electric double layer capacitance. The capacitive behavior of G/TiN NTA electrode was ascribed to fast electron transfer occurring on the intensified electrode surface of G/TiN NTA. The specific capacitance of G/TiN NTA electrode is obviously bigger than that of TiN NTA electrode at the same scan rate (Fig. 6C). The double electric layer of graphene and TiN NTA can storage more charge than only TiN NTA single electric layer.

A green thermal-reduction method at high-temperature was also used to reduce graphene oxide to graphene in order to study influences of different reduction methods on electrochemical performances. The thermal-reduction method needed enough temperature to cut off C-O bond totally. 600°C was selected as the thermal reduction temperature considering the stability of TiN NTA at high temperature. The experimental was done in a tube furnace under the protection of argon for four hours. Fig. 7 is the galvanostatic charge/discharge curves of G/TiN NTA, TRG/TiN NTA and G/NF electrodes at a current density of 4 A g<sup>-1</sup>. The specific capacitance of TRG/TiN NTA was 197.9 F g<sup>-1</sup>, which was lower than that of G/TiN NTA electrode. The main reason may be that 600°C was not high enough to cut off C-O bond of graphene oxide totally. So after reducing at 600°C, there was still survive of small port graphene oxide. Nevertheless, the specific capacitance of TRG/TiN NTA electrode was larger than that of G/NF electrode because TiN had higher conductivity and could supplied larger surface area than NF.



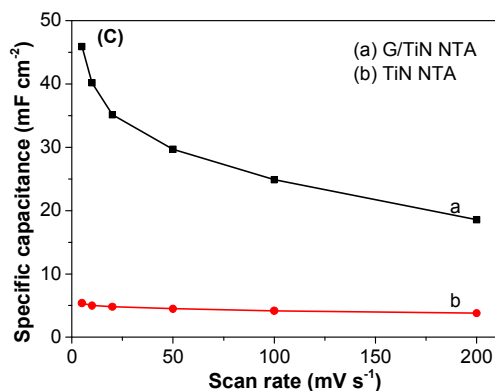


Fig. 6 (A, B) Cyclic voltammetry curves and (C) corresponding specific capacitance of TiN NTA and G/TiN NTA electrodes at different scan rates in 1.0 M KOH electrolyte solution.

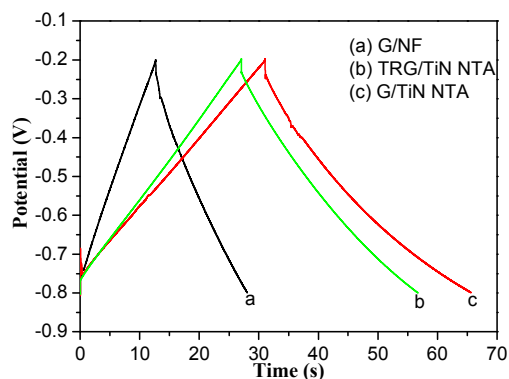


Fig. 7 Galvanostatic charge/discharge curves of (A) G/NF; (B) TRG/TiN NTA and (C) G/TiN NTA electrodes at a current density of 4 A g<sup>-1</sup>.

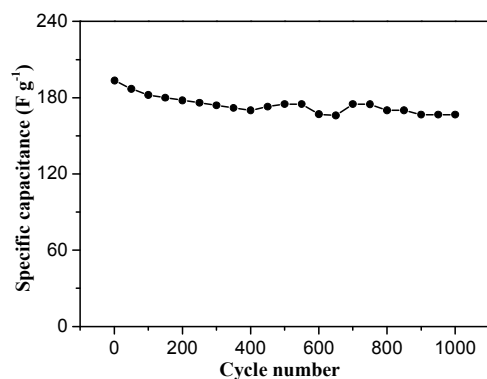


Fig. 8 Cycling performance of the G/TiN NTA electrode at a current density of 8.0 A g<sup>-1</sup>.

The cycling stability of the G/TiN NTA electrode was examined at a current density of 8.0 A g<sup>-1</sup> in 1.0 M KOH electrolyte. As shown in Fig. 8, the specific capacitance of G/TiN NTA electrode could maintain 86.1% after 1000 cycles. The stability reason ascribed to strong adsorption capacity between TiN NTA and graphene. The other reason was because of the framework of TiN NTA, which can slow down the active material graphene from collapsing

structurally.

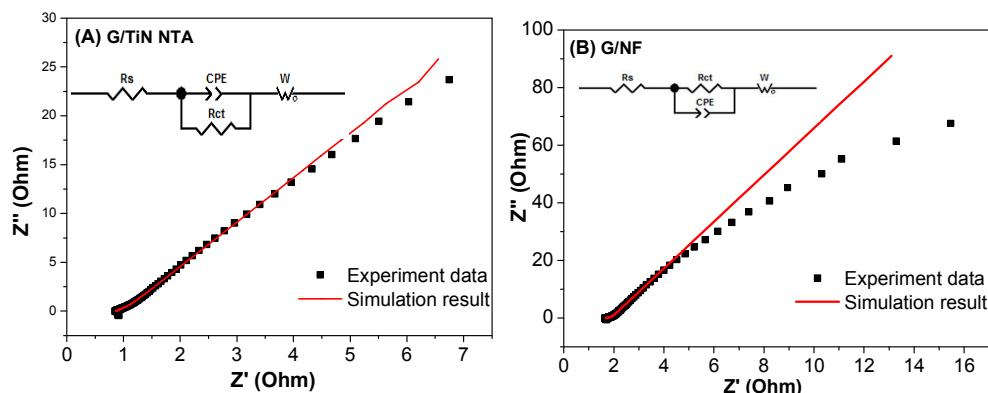


Fig. 9 Nyquist plot of EIS spectra and the corresponding equivalent circuit diagram of (A) G/TiN NTA and (B) G/NF electrodes in 1.0 M KOH electrolyte solution.

The enhanced electrochemical performance of the G/TiN NTA electrode was further confirmed by electrochemical impedance spectroscopy measurements. Fig. 9 shows the Nyquist plots of the electrochemical impedance spectroscopy of G/TiN NTA and G/NF electrodes. The corresponding equivalent circuit diagram was shown as the insert. An equivalent circuit was used to fit all elements, which consist of a bulk solution resistance  $R_s$ , a charge-transfer resistance  $R_{ct}$ , a Warburg resistance  $W$ , and a constant phase element CPE. The EIS spectra at high-frequency region were caused by a kinetics-controlled process and the beeline at a low-frequency region was caused by a diffusion-controlled process in the Nyquist plot. The slope of beelines related to the Warburg diffusion impedance was close to  $45^\circ$ , which demonstrated that the diffusion was the main factors affecting the whole process. Table 2 lists fitting results of the equivalent circuit diagram of G/TiN NTA and G/NF electrodes. As for G/TiN NTA, the value of  $R_s$  and  $R_{ct}$  are 0.86 and 0.15 Ohm, respectively. While as for G/NF, the value of  $R_s$  and  $R_{ct}$  are 1.65 and 0.24 Ohm, respectively. G/TiN NTA exhibited a smaller bulk solution resistance and charge-transfer resistance than that of G/NF electrode.

Table 2 Fitting results of the equivalent circuit diagram of G/TiN NTA and G/NF electrode.

Parameters	$R_s$	$R_{ct}$	W-R	W-P	W-T	CPE-T	CPE-P
Fitting value of G/TiN NTA (Ohm)	0.86	0.15	0	0.43	0	0.56	0.80
Fitting value of G/NF (Ohm)	1.65	0.24	0.28	0.01	0.46	0.10	0.96

Fig. 10A and B are the galvanostatic charge/discharge curves of G/TiN NTA and TiN NTA supercapacitor in the same potential range from -0.9 to 0.9 V at different specific current densities.

All charge–discharge curves are linear and symmetrical at various current densities, which was another typical characteristic of an ideal supercapacitor<sup>42</sup>. The specific capacity of G/TiN NTA and TiN NTA supercapacitor reached  $47.8 \text{ mF cm}^{-2}$  and  $15.6 \text{ mF cm}^{-2}$  at a current density of  $1 \text{ mA cm}^{-2}$ . It is certificated that graphene played an important role in enhancing the specific capacity of supercapacitor. Fig. 10C is the Ragone plot of G/TiN NTA supercapacitor. The working voltage was highly increased up to 1.8 V due to using gel polymer electrolyte instead of aqueous electrolyte. The corresponding energy storage properties are listed in Table 3. As the area current density increases, both area energy density and specific capacitance of this supercapacitor were slightly declined, but the area power density had a proportional increase. According to the initial voltage drop in the discharging profile, the internal resistance of this supercapacitor was determined to be  $8.3 \Omega$ .

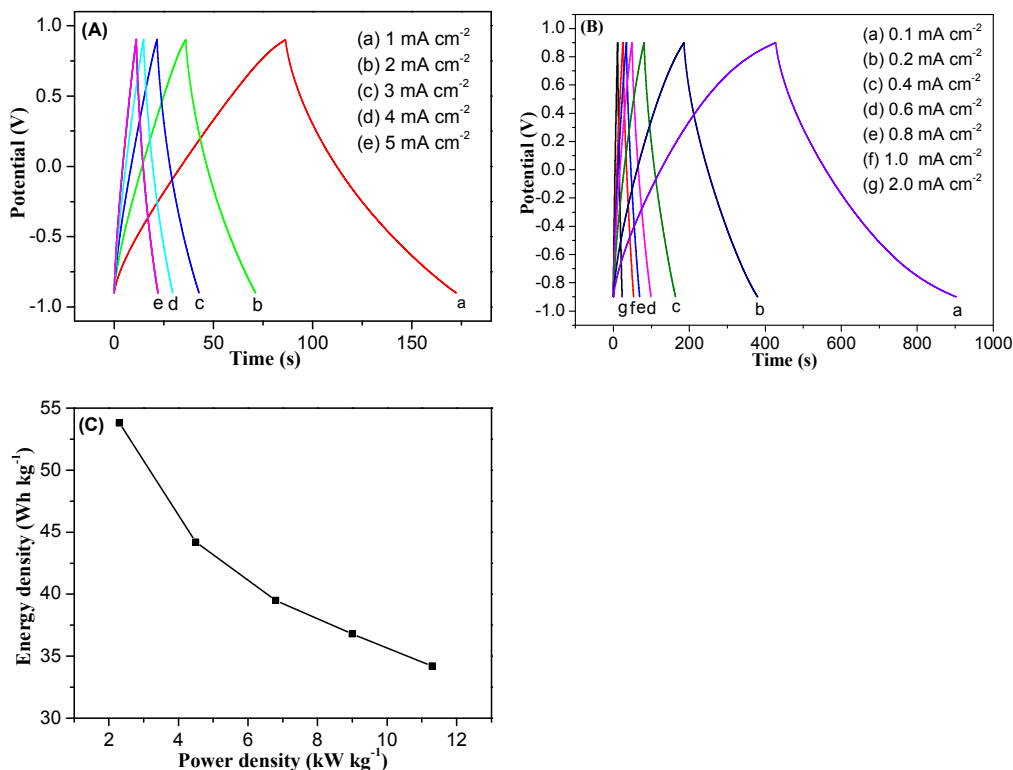


Fig. 10 Galvanostatic charge/discharge curves of (A) G/TiN NTA and (B) TiN NTA supercapacitors; (C) Ragone plots of G/TiN NTA supercapacitor.

Table 3 Specific capacitance, energy density and power density of all-solid state supercapacitor of G/TiN NTA at different current densities.

Current density ( $\text{mA cm}^{-2}$ )	1	2	3	4	5
Specific capacitance ( $\text{F g}^{-1}$ )	119.5	98.3	87.8	81.8	76.0

Energy density ( $\text{Wh kg}^{-1}$ )	53.8	44.2	39.5	36.8	34.2
Power density ( $\text{kW kg}^{-1}$ )	2.3	4.5	6.8	9.0	11.3

Nowadays, wearable electronic devices were becoming more fashionable compared with traditional electronics technology. Fig. 11A is a photograph of flexible G/TiN NTA supercapacitor. In order to verify the feasibility of our G/TiN NTA supercapacitor, we charged the supercapacitor and then found that the flexible supercapacitor could well power a light-emitting diode (Fig. 11B).

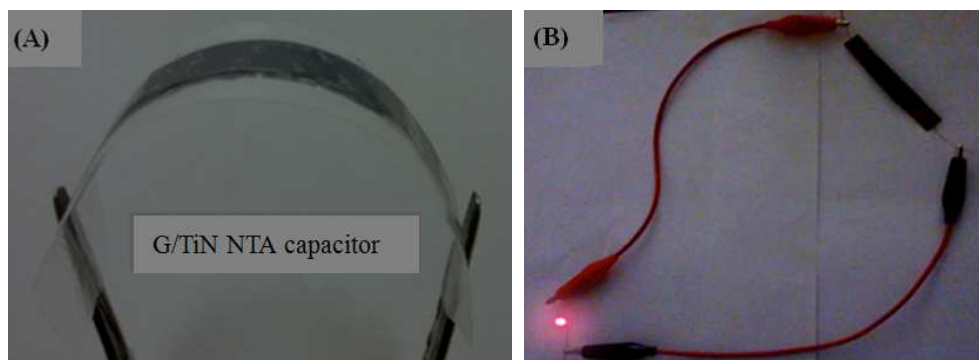


Fig. 11 Photographs of (a) G/TiN NTA flexible supercapacitor and (b) lighting a light-emitting diode

## 4 Conclusions

G/TiN NTA and G/NF composite electrode materials were synthesized by simple adsorption-reduction process. The G/TiN NTA shows a better capacitance performance than G/NF because TiN NTA could supply large surface area for graphene adsorption and feasible nanotube channels for electron transport. Both the chemical reduction method and the thermal reduction method were used to convert graphene oxide into graphene in order to investigate electrochemical performances of graphene electrodes. G/TiN NTA produced by chemical reduction method exhibited higher capacitance than TRG/TiN NTA produced by thermal reduction method. The G/TiN NTA electrode exhibited a specific capacitance of  $333.67 \text{ F g}^{-1}$  at a current density of  $1.0 \text{ A g}^{-1}$  in  $1.0 \text{ M KOH}$  electrolyte solution and kept 86.1 % capacity retention after 1000 cycles. An all-solid state supercapacitor was also assembled using two symmetric electrodes of G/TiN NTA and polyvinyl alcohol-potassium hydroxide-potassium iodide gel electrolyte. The specific capacity of G/TiN NTA supercapacitor reached  $76.0 \text{ F g}^{-1}$  at a current density of  $5 \text{ mA cm}^{-2}$ . The all-solid state supercapacitor exhibited energy density of  $34.2 \text{ Wh kg}^{-1}$  and power density of  $11.3 \text{ kW kg}^{-1}$ .

It shows the possibility of G/TiN NTA to act as electrode material of supercapacitors.

## Acknowledgements

This work was supported by National Natural Science Foundation of China (No. 21373047 and 20871029), Program for New Century Excellent Talents in University of the State Ministry of Education (No. NCET-08-0119) and Science & Technology Program of Suzhou City (No. ZXG2012026, SYN201208 and SYG201017).

## References

- 1 Y. Wang, Z. S. Feng, C. Zhang, L. Yu, J. J. Chen, J. Hu and X. Z. Liu, *Nanoscale*, 2013, **5**, 3704-3712.
- 2 Y. Wang, Z. S. Feng, J. J. Chen and C. Zhang, *Mater. Lett.*, 2012, **71**, 54-56.
- 3 Y. Xie and H. Du, *J. Solid State Electrochem.*, 2012, **16**, 2683-2689.
- 4 A. K. Geim and K. S. Novoselov, *Nature Mater.*, 2007, **6**, 183-191.
- 5 H. Q. Wu, C. Y. Linghu, H. M. Lu and H. Qian, *Chin. Phys. B*, 2013, **22**.
- 6 C. N. R. Rao, A. K. Sood, K. S. Subrahmanyam and A. Govindaraj, *Angew. Chem.-Int. Edit.*, 2009, **48**, 7752-7777.
- 7 M. J. Allen, V. C. Tung and R. B. Kaner, *Chem. Rev.*, 2010, **110**, 132-145.
- 8 D. A. Dikin, S. Stankovich, E. J. Zimney, R. D. Piner, G. H. B. Dommett, G. Evmenenko, S. T. Nguyen and R. S. Ruoff, *Nature*, 2007, **448**, 457-460.
- 9 M. S. Fuhrer, *Science*, 2013, **340**, 1413-1414.
- 10 X. W. Yang, C. Cheng, Y. F. Wang, L. Qiu and D. Li, *Science*, 2013, **341**, 534-537.
- 11 P. C. Lian, X. F. Zhu, H. F. Xiang, Z. Li, W. S. Yang and H. H. Wang, *Electrochim. Acta*, 2010, **56**, 834-840.
- 12 W. Wang, Y. Xie, Y. Wang, H. Du, C. Xia and F. Tian, *Microchim. Acta*, 2014, **181**, 381-387.
- 13 Y. Xie and Y. Zhao, *Mater. Sci. Eng., C*, 2013, **33**, 5028-5035.
- 14 D. Choi and P. N. Kumta, *J. Electrochem. Soc.*, 2006, **153**, A2298-A2303.
- 15 S. M. Dong, X. A. Chen, L. Gu, X. H. Zhou, H. X. Xu, H. B. Wang, Z. H. Liu, P. X. Han, J. H. Yao, L. Wang, G. L. Cui and L. Q. Chen, *Acs Appl. Mater. Interface*, 2011, **3**, 93-98.

- 16 X. H. Lu, G. M. Wang, T. Zhai, M. H. Yu, S. L. Xie, Y. C. Ling, C. L. Liang, Y. X. Tong and Y. Li, *Nano Lett.*, 2012, **12**, 5376-5381.
- 17 Y. Xie and X. Fang, *Electrochim. Acta*, 2014, **120**, 273-283.
- 18 C. Xia, Y. Xie, Y. Wang, W. Wang, H. Du and F. Tian, *J. Appl. Electrochem.*, 2013, **43**, 1225-1233.
- 19 P. X. Han, Y. H. Yue, X. G. Wang, W. Ma, S. M. Dong, K. J. Zhang, C. J. Zhang and G. L. Cui, *J. Mater. Chem.*, 2012, **22**, 24918-24923.
- 20 H. Du, Y. Xie, C. Xia, W. Wang and F. Tian, *New J. Chem.*, 2014, **38**, 1284-1293.
- 21 Y. Xie, Y. Wang and H. Du, *Mater. Sci. Eng., B*, 2013, **178**, 1443-1451.
- 22 W. S. Hummers and R. E. Offeman, *J. Am. Chem. Soc.*, 1958, **80**, 1339-1339.
- 23 Y. Xu, L. Zhao, H. Bai, W. Hong, C. Li and G. Shi, *J. Am. Chem. Soc.*, 2009, **131**, 13490-13497.
- 24 K. Zhang, L. L. Zhang, X. S. Zhao and J. S. Wu, *Chem. Mater.*, 2010, **22**, 1392-1401.
- 25 L. Sun, H. Yu and B. Fugetsu, *J. Hazard. Mater.*, 2012, **203**, 101-110.
- 26 H. Y. Yu, J. H. Wu, L. Q. Fan, K. Q. Xu, X. Zhong, Y. Z. Lin and J. M. Lin, *Electrochim. Acta*, 2011, **56**, 6881-6886.
- 27 S. Giri, D. Ghosh and C. K. Das, *J. Electroanal. Chem.*, 2013, **697**, 32-45.
- 28 I. Jung, D. A. Dikin, R. D. Piner and R. S. Ruoff, *Nano Lett.*, 2008, **8**, 4283-4287.
- 29 W. Spengler, R. Kaiser, A. N. Christensen and G. Mullervogt, *Phys. Rev. B*, 1978, **17**, 1095-1101.
- 30 Y. H. Yue, P. X. Han, X. He, K. J. Zhang, Z. H. Liu, C. J. Zhang, S. M. Dong, L. Gu and G. L. Cui, *J. Mater. Chem.*, 2012, **22**, 4938-4943.